# SIMPLE AND COMPACT LINEAR-MOTION GUIDANCE

**The performance of electrical actuators is typically limited by the ohmic losses, which cause heat generation. This not only compromises thermal stability needed in precision applications but can also lead to overheating. This challenge can be addressed by using superconductors in the actuator's coil to eliminate electrical resistance. This article presents the design of a compact superconducting voice-coil actuator that delivers a high static force of 350 N while generating only 1 mW of heat. The incorporated spiral diaphragm flexures offer a simple and compact solution to guide the linear motion.**

KOEN DWARSHUIS, KOEN VAN GINKEL, WOUTER VERBRUGGEN, GONÇALO SANTOS TOMÁS, MARC DHALLÉ, MATHIJS VAN GORCUM, BAS DE VRIES, MATTHIJS NEUT, JAAP BRAND, RAYMOND BOERSMA, DANNIS BROUWER AND HANS VAN OORT

## Introduction

The high-tech industry increasingly demands more powerful electrical actuators. However, the maximum achievable actuation force is often limited by ohmic losses in the coil, which results in heat generation. Higher forces typically necessitate larger actuators and a higher cooling capacity. Additionally, heat generation compromises thermal stability and must therefore be minimised in high-precision applications. Incorporating superconducting materials in the coil can substantially reduce ohmic losses, offering a promising solution.

Superconductivity is typically achieved in cryogenic environments, which presents significant challenges for motion guidance. Conventional roller or slider bearings are unsuitable due to ineffective lubrication, dimensional changes during cool-down, and the risk of ice formation. Flexures provide an effective solution, and their predictable mechanical behaviour makes them also suitable for high-precision applications.

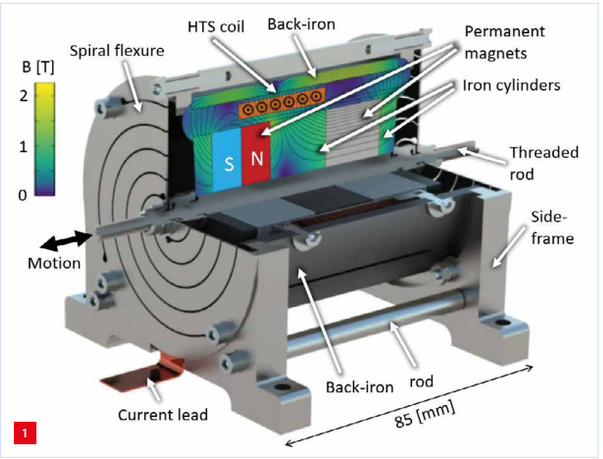


*Actuator design, with the magnetic field introduced by the permanent magnets and a current of 20 A in the coil.*

High-temperature superconductors (HTS) have been applied since about 1990, primarily in large-scale rotational actuators [1]. This article presents the design of a compact linear superconducting actuator providing high static actuation force. The coil is wound from commercially available ReBCO-tape (rare-earth barium copper oxide). The moving component is guided by a pair of spiral diaphragm flexures. It offers a 10 mm range of motion within a cylindrical footprint of approximately ø75 x 90 mm$^3$. The actuator is cooled within liquid nitrogen, so the operational temperature is 77 K. The electromagnetic part of the actuator is also described in [2].

## Actuator design

A voice-coil actuator generates force between a stator and a moving part. One part comprises permanent magnets to generate a magnetic field, the other part a coil. This generates a Lorentz force between both parts, which, for a small segment of wire in the coil, can be expressed as:

$$F = l\,(\boldsymbol{I} \times \boldsymbol{B}) \qquad (1)$$

Here, $l$ is the length of the wire in the coil, $\boldsymbol{I}$ the current in the wire, and $\boldsymbol{B}$ the magnetic field.

Figure 1 illustrates the current voice-coil actuator design. The moving part comprises two permanent magnets positioned between three iron cylinders, all mechanically lined by a threaded rod. Their motion is enabled by two spiral diaphragm flexures. The stationary coil is bolted to the tubular back-iron and features copper current leads on both ends. Side frames are attached to either end of the back-iron, also serving as mounting point for the flexures. The entire frame is held together by three rods.

**AUTHORS' NOTE**

Koen Dwarshuis, Koen van Ginkel and Dannis Brouwer are associated with the chair of Precision Engineering in the Faculty of Engineering Technology at the University of Twente (UT) in Enschede (NL).

Wouter Verbruggen Gonçalo Santos Tomás, Marc Dhallé and Hans van Oort are associated with the chair of Energy, Materials & Systems in the Faculty of Science and Technology at the UT.

Koen van Ginkel, Mathijs van Gorcum, Bas de Vries, Matthijs Neut, Jaap Brand and Raymond Boersma are associated with VDL ETG Technology & Development in Almelo (NL).

**k.s.dwarshuis@utwente.nl**
**www.utwente.nl/en/et/ms3**
**www.utwente.nl/en/tnw/ems**
**www.vdletg.com**

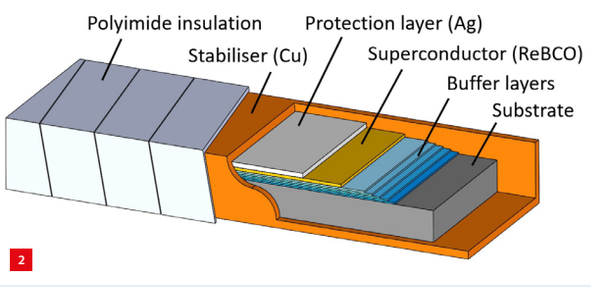


*ReBCO-tape; layers not to scale.*

*Coil*

The coil is wound using ReBCO-tape (Figure 2), which consists of superconducting material deposited on a substrate and surrounded by a copper stabiliser. The tape is electrically insulated with a polyimide wrap. Most ReBCO-based coils adopt a pancake layout (Figure 3a), typically comprising multiple serially stacked sub-coils wound alternatingly in clockwise and counterclockwise directions. This configuration requires electrical joints between sub-coils, which are mechanically and electrically vulnerable, introduce ohmic losses, and are challenging to fabricate.

For the actuator presented here, a solenoid layout was chosen (Figure 3b), eliminating the need for intermediate joints. However, this type of winding introduces a lot of extra strain in the superconducting layer of the tape, while excessive strain (typically beyond 0.45% in tension or 1.3% in compression) harms the superconducting properties.

As with the pancake layout, out-of-plane bending of the tape is required during winding, introducing strain in the superconducting layer. In the solenoid layout, additional in-plane bending occurs during layer transitions, as this requires the winding angle to be inverted. The maximum resulting strain is approximately proportional to the square of the ratio between the width of the tape and the coil radius: $\varepsilon \approx 0.5(w/\pi r)^2$. To mitigate this effect, a narrow tape width of 2 mm was selected.

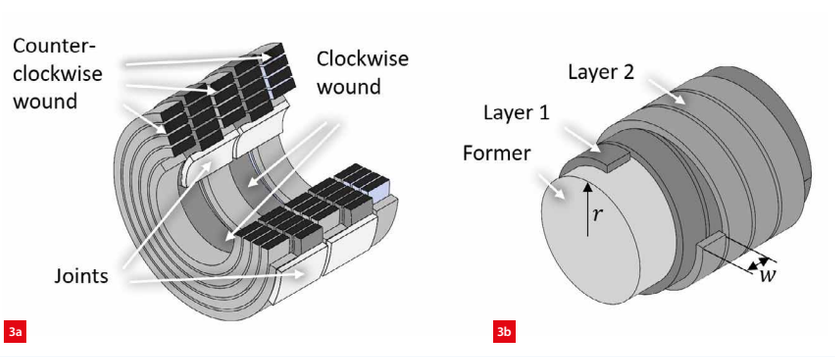


*Coil layouts.*
*(a) Pancake.*
*(b) Solenoid.*

**Table 1**
Properties of the ReBCO solenoid coil.

| Description | Value |
|---|---|
| Tape width | 2 mm |
| Tape thickness | 0.1 mm |
| Inner radius | 44 mm |
| Outer radius | 50.5 mm |
| Number of tape layers | 21 |
| Total number of turns | 198 |

The tape is wet-wound onto the former with Stycast 2850FT epoxy, which offers thermal contraction similar to the tape and provides good thermal conductivity. The resulting coil specifications are summarised in Table 1.

*Permanent magnets*

The moving assembly was designed to produce a permanent magnetic field that is, ideally, radial within the coil. This orientation maximises the actuation force, see the cross-product in Equation 1. This is accomplished using a semi-Hallbach layout: two magnets are oriented with their north pole facing inward, toward the centre, and are placed between iron cylinders. The back-iron serves to steer the magnetic field around the coil in the radial direction. Figure 1 shows the resulting simulated magnetic field. It is not symmetric across the *xy*-plane as it also includes the current-induced magnetic field generated by the coil.

## Flexure design

The moving part is guided by two spiral diaphragm flexures that constrain radial translation and rotation around the *x*-axis (Figure 4a). Each spiral diaphragm consists of multiple flexure arms in parallel. With motion in the *x*-direction, the shortening of these flexure arms causes a small rotation of the mover around the *x*-axis. However, this rotation does not affect the actuator's performance because of rotational symmetry.

The flexures should provide sufficient radial support stiffness to counteract the magnetic attraction between the magnetic mover and the back-iron when the mover is slightly off-centred. Magnetostatic simulations indicated that a minimum support stiffness of 120 N/mm is required. Additionally, the axial actuation stiffness should be as low as possible, such that this does not significantly reduce the actuation force during displacement.

To evaluate the spiral diaphragm flexure, it was compared against two alternative linear flexure guidance concepts, as illustrated in Figure 4. The six-fold concept consists of two sets of three folded leafsprings, of which one side is tapered.

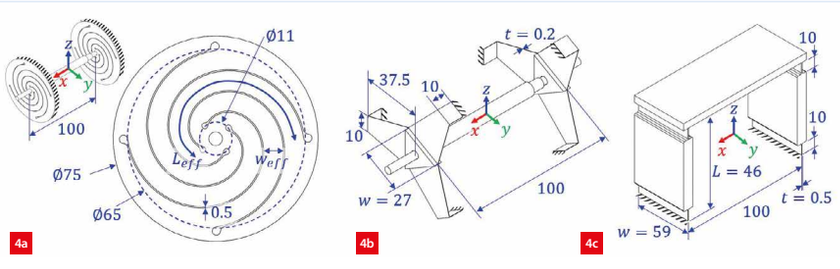


*Flexure guidance concepts for linear motion; dimensions in [mm].*
*(a) Spiral diaphragms.*
*(b) Six-fold leafsprings.*
*(c) Reinforced leafsprings.*

The third concept features two reinforced leafsprings. All three designs incorporate two flexure sets that constrain motion in the $y$-, $z$- and $R_x$-directions, resulting in an over-constrained system in $R_x$-direction.

Each concept was optimised for support stiffness in the $y$-direction. The flexural parts were modelled as Ti-6Al-4V titanium alloy, characterised by a Young's modulus of 107 GPa and a Poisson's ratio of 0.29. They must accommodate the full ±5 mm translational motion, without exceeding a maximum allowable stress of 500 MPa. They should fit within a cylindrical build volume of ø75 x 100 mm$^3$. The design optimisations were performed in Ansys, where the flexures were modelled using quadratic shell elements and the frame parts were treated as rigid bodies.

The dimensions of the three concepts are shown in Figure 4 and detailed as follows:

- Spiral diaphragms: the cut-outs are Archimedean spirals with outer and inner diameters of 65 mm and 11 mm, respectively, and a gap width of 0.5 mm. Variants with 3, 4 and 5 flexure arms were explored. The only optimised parameters were the thickness (varied in 0.1-mm increments) and the number of revolutions of each of these cut spirals. A higher number of revolutions increases the effective length of the arms, while reducing the effective width. This change lowers the maximum material stress and the required actuation force, but it also reduces the support stiffness. Table 2 lists the design parameters, together with the resulting effective length and width of the arms.

**Table 2**
Dimensions of the optimised spiral flexure.

| Number of arms | Thickness [mm] | Number of revolutions | $L_{eff}$ [mm] | $w_{eff}$ [mm] |
|---|---|---|---|---|
| 3 | 0.8 | 0.97 | 76 | 8.8 |
| 4 | 0.8 | 0.85 | 72 | 7.4 |
| 5 | 0.7 | 0.75 | 66 | 6.7 |

- Six-fold leafsprings: the radial distance from the centre to the flexure folds was 37.5 mm, ensuring the design nearly remains in the allowable build volume. The width of one side of the tapered part was fixed to 10 mm and the other side's width was optimised, resulting in a value of 27 mm. The thickness of the flexures, varied in 0.1-mm increments, was found to be 0.2 mm in the best-performing configuration.
- Reinforced leafsprings: the length and width of the flexures were optimised under the constraint that the diagonal was 75 mm, given by the relation $\sqrt{(L^2 + w^2)} = 75$ mm. The thickness of the flexures was the last optimisation parameter. The length of the compliant regions was fixed at 10 mm; optimising this length would result in infinitely short and thin flexures.

Figure 5 shows that the reinforced leafspring concept clearly outperforms the others in terms of support stiffness, but it has a high required actuation force. However, halving the flexure thickness significantly reduces the actuation force – making it the lowest among all concepts – while still maintaining a high level of support stiffness. A drawback of this design is the parasitic motion in the $z$-direction, caused by the shortening of the flexures. For the current geometry and 5 mm displacement, this motion is approximately 0.3 mm.

The six-fold flexure exhibits the lowest support stiffness of the three concepts. This is due to the short effective length of its leafsprings, which requires limiting the thickness to 0.2 mm to stay within the 500 MPa stress constraint.

The spiral diaphragm concepts also show relatively low support stiffness. This is primarily due to the need for long, narrow flexure arms to allow the required ±5 mm travel, resulting in low bending support stiffness. Among the spiral variants, the design with four arms provides the highest support stiffness at the end of the motion range, indicating it is the most favourable configuration under the given design constraints.

All three concepts meet the minimum required support stiffness of 120 N/mm, making them technically suitable. The spiral diaphragm was selected because of its manufacturing simplicity and compact build volume.

## Experiments

Figure 6 shows the realised mechanism, which for reasons of practicality and proper comparison deviates somewhat from the above-described optimised design. The spiral flexure in the realised prototype has modified dimensions to reduce stiffness in the actuation direction. This also decreases the support stiffness, but it is still well above the required 120 N/mm.

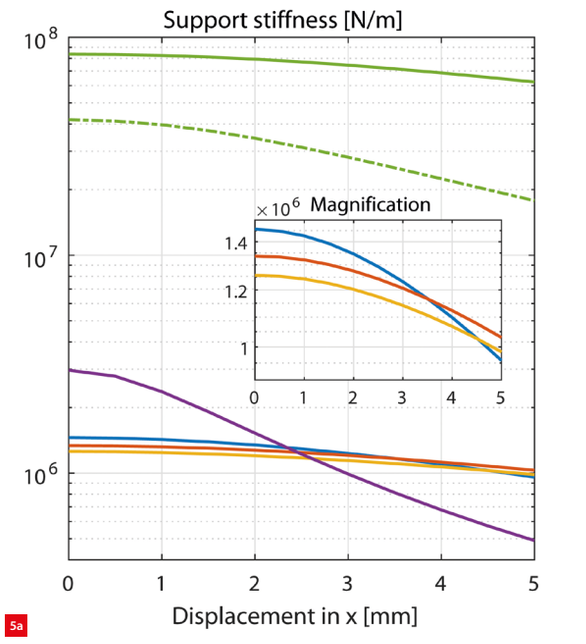


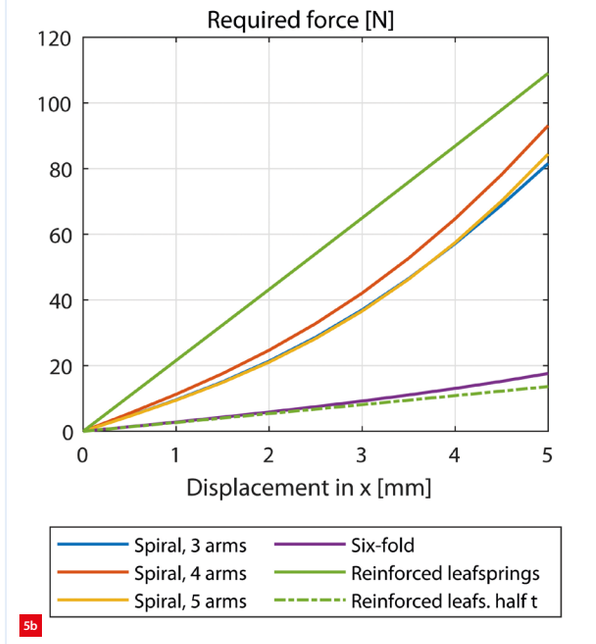


*Performance of the optimised flexure concepts.*
*(a) Support stiffness.*
*(b) Actuation force.*

*Mechanical experiment*

To assess the stiffness of the flexures, the eigenmodes of the mechanism were experimentally measured. Vibrations were induced using a speaker and captured with a laser vibrometer; see Figure 7. These were compared with results from a finite-element model (FEM) of the flexures and mover. In the model, the mass of the mover was matched to the measured value of 0.675 kg. To account for the magnetic attraction between the mover and the back-iron, the model contained mechanical springs that introduced a stiffness of 1.2 N/mm in the actuation direction and a negative stiffness of 120 N/mm in the radial direction; these values were obtained with magnetostatic simulations.

Figure 8 presents the simulated mode shapes and the corresponding experimental and simulated eigenfrequencies. The comparison shows some differences between the experimental and FEM results, which can be attributed to inaccuracies in the modelled magnetic attractions and deviations in the actual thickness of the fabricated spiral flexures.

*Electrical measurement*

The electrical resistance of the coil was measured as a function of the applied current; see Figure 9. A key performance indicator is the critical current: the point

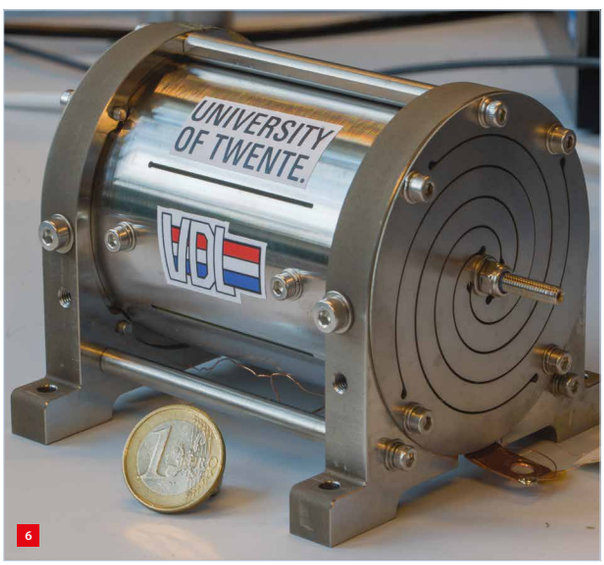


*Realised actuator.*

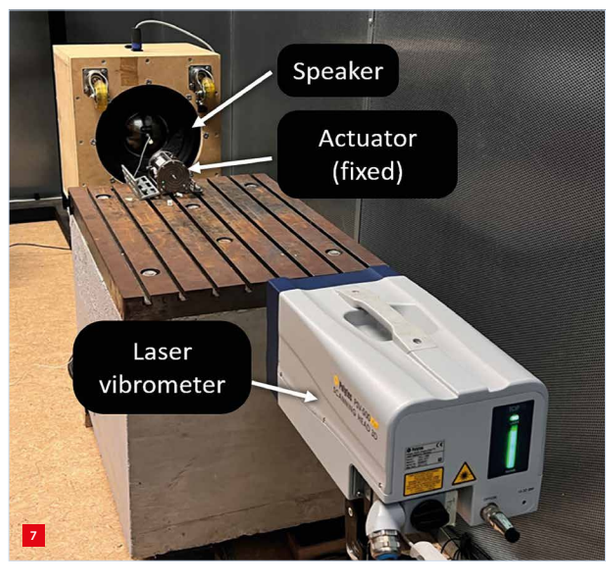


*Experimental set-up for measuring eigenmodes.*

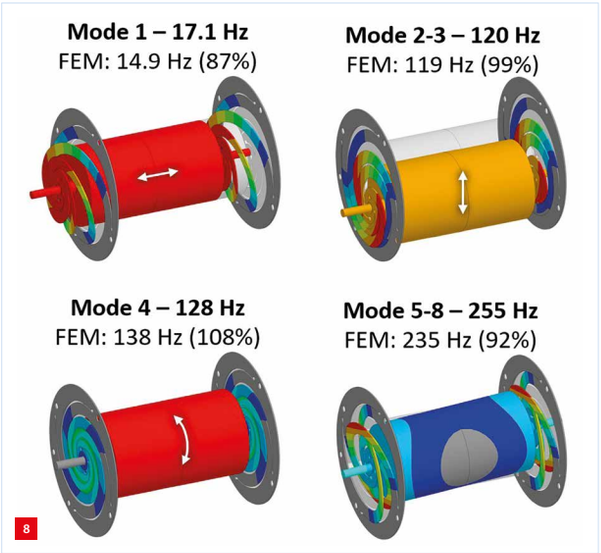


*Eigenmodes; the text shows experimentally obtained frequencies and their relative agreement with FEM results. Because of cyclic repetition, modes 2 and 3 are equal, and similarly modes 5 to 8 are equal.*

at which a conductor loses its superconducting properties. This is typically defined by a voltage drop exceeding 100 µV/m. Using this criterium, the fitted power law indicated a critical current of 32.6 A, slightly higher than the value predicted from Robinson Institute's HTS database [3]. With a current of 26 A, the heat loss remained less than 1 mW. The measurement was also performed with the coil outside the actuator, yielding a critical current that was approximately twice as high. This is because the additional magnetic field of the permanent magnets significantly decreases the superconducting properties of the ReBCO-tape.

*Force measurement*

The generated force was measured as a function of the current with the actuator in its neutral position. A custom S-type load cell, equipped with cryogenically compatible strain gauges, was used for this purpose. Figure 10 shows

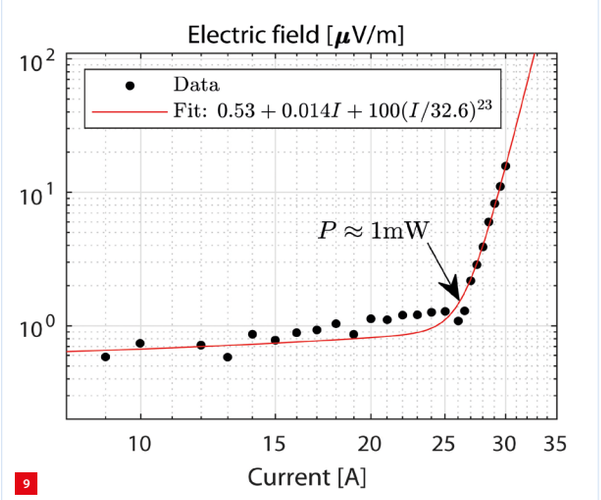


*Current-voltage plot of the ReBCO coil inside the actuator.*

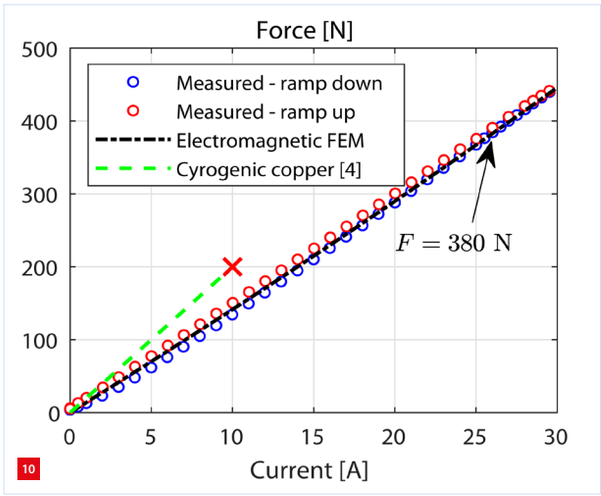


*Measurement of the force produced by the actuator.*

that the actuator produced a force of 350 N at the maximum operational current of 26 A. This performance significantly exceeds that of a comparable actuator using a copper-wire coil at cryogenic temperatures, which achieves a maximum actuation force of approximately 200 N, while generating approximately 10 W of heat [4].

## Conclusions and outlook

The design of the small actuator based on ReBCO tape demonstrates that a static force of 350 N can be reached with less than 1 mW heat dissipation. The spiral diaphragm flexure provides sufficient support stiffness and offers manufacturing simplicity, making it a suitable guidance.

In future research, the dynamic performance will be tested and the temperature distribution in the coil will be measured. Furthermore, a new actuator will be designed, conduction-cooled using a cryo-cooler instead of liquid nitrogen. This makes the actuator compatible with vacuum environments and it may enable operation at lower temperatures, thereby significantly enhancing the performance of the superconducting tape. In this way, the potential of superconducting actuators can be even further enhanced, enabling larger actuation forces at lower heat dissipation in smaller volumes.

REFERENCES

[1] C.C.T. Chow, M.D. Ainslie, and K.T. Chau, "High temperature superconducting rotating electrical machines: An overview", *Energy Reports*, vol. 9, pp. 1124-1156, 2023.
[2] W.M. Verbruggen, *et al.*, "A compact & efficient linear actuator based on a layer-wound ReBCO solenoid", *Supercondonductor Science and Technology*, 2025, submitted.
[3] S.C. Wimbush, Robinson HTS wire critical current database, *htsdb.wimbush.eu*, accessed 5 March 2025.
[4] M.J. Naus, "Design of a superconducting voice coil actuator", technical report, VDL ETG Technology & Development and University of Twente, 2021.